IOP PUBLISHING
JOURNAL OF PHYSICS B: ATOMIC, MOLECULAR AND OPTICAL PHYSICS
J. Phys. B: At. Mol. Opt. Phys. **42** (2009) 061001 (5pp)
doi:10.1088/0953-4075/42/6/061001

FAST TRACK COMMUNICATION

Origin of species dependence of high-energy plateau photoelectron spectra

Zhangjin Chen[1], Anh-Thu Le[1], Toru Morishita[2,3] and C D Lin[1]

[1] J R Macdonald Laboratory, Physics Department, Kansas State University, Manhattan, KS 66506-2604, USA
[2] Department of Applied Physics and Chemistry, University of Electro-Communications, 1-5-1 Chofu-ga-oka, Chofu-shi, Tokyo 182-8585, Japan
[3] PRESTO, JST Agency, Kawaguchi, Saitama 332-0012, Japan

Received 22 October 2008, in final form 18 January 2009
Published 9 March 2009
Online at stacks.iop.org/JPhysB/42/061001

Abstract
We analysed the energy and momentum distributions of high-energy 'plateau' photoelectrons. These electrons, with energies above $4U_p$ (U_p is the ponderomotive energy), have been understood qualitatively as due to the backscattering of laser-induced returning electrons by the target ion. Here, we establish a quantitative rescattering (QRS) theory to show that the species and laser-intensity dependence of the 'flatness' of the plateau electrons is *entirely* determined by the energy and angular dependence of the elastic scattering cross sections between target ions with *free* electrons. This accurate QRS theory can be used to obtain energy and momentum distributions of plateau electrons without the need of solving the time-dependent Schrödinger equation.

(Some figures in this article are in colour only in the electronic version)

When atoms or molecules are placed in an intense laser pulse, an electron can be released through either a multiphoton or a tunnelling mechanism. The distinction is based on the Keldysh parameter $\gamma = \sqrt{I_p/2U_p}$, where I_p is the ionization energy, $U_p = A_0^2/4$ (atomic units are used unless otherwise specified) is the ponderomotive energy and A_0 is the peak value of the vector potential. In the multiphoton regime ($\gamma > 1$), the electron spectra exhibit characteristic above-threshold ionization (ATI) peaks separated by photon energy, with yields decreasing monotonically with increasing electron energy [1]. At higher intensities, in the tunnelling region ($\gamma < 1$), the spectra are notably different. First, the ionization yield drops steeply from the threshold, but from about 3 or $4U_p$ onwards, the yield flattens out significantly until about $10U_p$ where it drops precipitously again. The flattened spectral region from 4 to $10U_p$ is called the plateau electrons. Despite this common description, electron spectra in the plateau region are not always flat. The flatness depends on the species and laser intensity. For example, experimental ATI spectra for potassium show strong enhancement in the plateau region, but not for sodium [2]. Similarly, using nearly identical lasers, a clear flat plateau shows up in an Xe target, but not in Kr and Ar [3]. Experimentally, the flatness of plateau electrons has been observed to depend on laser intensities [4] as well.

Experimentally, the plateau photoelectrons in ATI spectra from atoms have been studied since 1990s [5–7]. Qualitatively, they are understood based on the rescattering model [8–11]. In this model, electrons that are released earlier by tunnelling ionization can be driven back by the laser field to recollide with the target ion. The plateau electrons are due to elastic large-angle backscattering of the returning electrons by the target ion. Quantitatively, accurate high-energy electron spectra rely on computations carried out by solving the time-dependent Schrödinger equation (TDSE) within the single active electron approximation [12, 13]. However, these theories do not offer the interpretation for the origin of species and laser-intensity dependence of the flatness of plateau electrons. In this communication, we present a *quantitative* rescattering theory (QRS) which shows that the species and laser-intensity dependence of plateau electrons is determined *entirely* by the electron–ion elastic scattering differential cross sections (DCSs) at large angles. Although such a relation has been

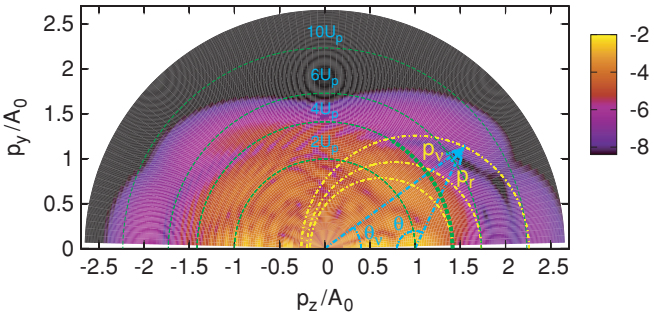

Figure 1. Typical 2D electron momentum distribution (in logarithmic scale). The *photoelectrons* of a given energy are represented on a concentric circle centred at the origin. The elastic scattering of a returning electron with momentum p_r in the laser field is represented by a partial circle with its centre shifted from the origin by $A_r = p_r/1.26$. High-energy plateau electrons are obtained via large-angle backscattering only. See text.

discussed previously [2, 7], direct quantitative connection between the two has never been established so far.

To understand the plateau electrons, we first examine their spectra in momentum space. In figure 1, we show typical two-dimensional (2D) electron momentum spectra. The horizontal axis is along the laser's polarization and the vertical axis is in any direction perpendicular to it (the electron spectra have cylindrical symmetry). In the figure, contour lines with photoelectron energies of 2, 4, 6 and $10U_p$ are shown. In addition, three circular arcs are drawn, each with its centre shifted from the origin. Consider the outermost arc; it has a radius p_r. Measured from its own centre, the circle represents the momentum surface of an elastically scattered electron with momentum $\vec{p}_r$. However, if collision occurs in the laser field at the instant when the vector potential is A_0, the electron will exit the laser field gaining an additional momentum $-A_0\hat{p}_z$, with photoelectron momentum $\vec{p}_v = -A_0\hat{p}_z + \vec{p}_r$. The outgoing angle θ_v and electron scattering angle θ, which is measured from the negative p_z direction, are shown in the figure. Note that only for large-angle backscattering can photoelectrons reach high energies, defined here to be above $4U_p$. The 2D spectra shown in figure 1 are calculated by solving the TDSE for a Na target, using a five-cycle, 3200 nm, linearly polarized laser, with a peak intensity of 10^{12} W cm^{-2}. The shape of the laser pulse is a cosine-squared function and the carrier-envelope phase is zero [14].

According to the classical theory, an electron that returns to the core with a maximum energy of $3.17U_p$, or a maximum momentum of $p_r = 1.26A_0$, will emerge with a kinetic energy of $10U_p$ if it is backscattered by 180° [6]. In a recent paper [15], we investigated the photoelectron momentum distributions of such electrons after they are backscattered by the ion at different angles. These electrons lie on the back rescattering ridge (BRR), i.e. along the outermost shifted arc in figure 1. It was shown that along the BRR, the photoelectron yield $I(p_v, \theta_v)$ is proportional to the electron–ion DCS, $\sigma(p_r, \theta)$:

$$I(p_v, \theta_v) = S(p_r)\sigma(p_r, \theta), \tag{1}$$

where $p_r = 1.26A_0$.

In order to verify equation (1), $I(p_v, \theta_v)$ was calculated by solving the TDSE [16] in the single active electron approximation. The atomic potential is expressed as $V(r) = -1/r + V_s(r)$, where V_s is the short-range potential that accounts for the screening of the nucleus by other passive electrons. The elastic scattering DCS, $\sigma(p_r, \theta)$, of an electron by such a potential $V(r)$ is treated in standard quantum mechanics textbooks; see e.g. [17]. Both $I(p_v, \theta_v)$ and $\sigma(p_r, \theta)$ for such a model problem can be calculated 'exactly'. If equation (1) is correct, then $S(p_r)$ derived from the ratio $I(p_v, \theta_v)/\sigma(p_r, \theta)$ should be independent of the scattering angle θ. This has been shown to be true for θ greater than about 100°. The validity of equation (1) along the BRR has since been confirmed in two recent experiments [18, 19], where electron–ion DCSs were extracted from laser-induced photoelectron momentum spectra for rare gas atoms.

In [15], the validity of equation (1) has been established for $p_r = 1.26A_0$ only. This limits its usefulness for studying high-energy photoelectrons. To examine plateau electrons with energies from $4U_p$ to about $10U_p$, elastic scattering by electrons with returning energies less than $3.17U_p$, or momenta $p_r < 1.26A_0$, must be included. According to the semiclassical theory [20], for lower energies, electrons will return to the core at two different times, t_1 and t_2, following short and long trajectories, respectively. Neglecting the small differences in the vector potentials and in the returning electron momenta at the two return times, we can retain the simplicity of equation (1) for the $p_r < 1.26A_0$ region where the 'wave packet' $S(p_r)$ now contains interference from the two elastic collisions at t_1 and t_2. To use equation (1), we also need to establish the relation between p_r and A_r. We set $p_r = 1.26A_r$, similar to that for BRR electrons, since plateau electrons result from the backscattering of returning electrons with energies close to $3.17U_p$. With this generalization, we obtain the QRS model. We establish its region of validity by comparing with results obtained from TDSE calculations, as shown below.

To test the QRS model in the 4–$10U_p$ region, we first show in figures 2(a) and (b) the electron momentum spectra ($p_z \geqslant 0$) for sodium and potassium atoms. On the left-hand half of the 2D plot, the results from the TDSE are shown, and on the right-hand half the same distributions from the QRS model are given. If the QRS model is accurate, then each plot should exhibit good reflection symmetry. This is clearly the case for each target, showing the validity of the QRS model. To obtain QRS results, we first evaluate the 'wave packet' $S(p_r)$ using $S(p_r) = I(p_v, \theta_v)/\sigma(p_r, \theta)$ at an arbitrary scattering angle, say $\theta = 170°$, where $I(p_v, \theta_v)$ is extracted from the TDSE results and $\sigma(p_r, \theta)$ is calculated using the standard potential scattering theory [17]. Once $S(p_r)$ is obtained, the whole 2D electron momentum spectra for photoelectrons with energies above $4U_p$ can be 'reproduced' from equation (1) by calculating $\sigma(p_r, \theta)$ for other scattering angles. From figure 1, it is clear that θ is limited to large angles only for this high-energy region. We will later show (in figure 3(b)) that $S(p_r)$ depends mostly on the lasers only. Thus according to the QRS model, all the structure information about plateau electrons in ATI is contained in the DCS, $\sigma(p_r, \theta)$, between the returning electrons and the target ion.

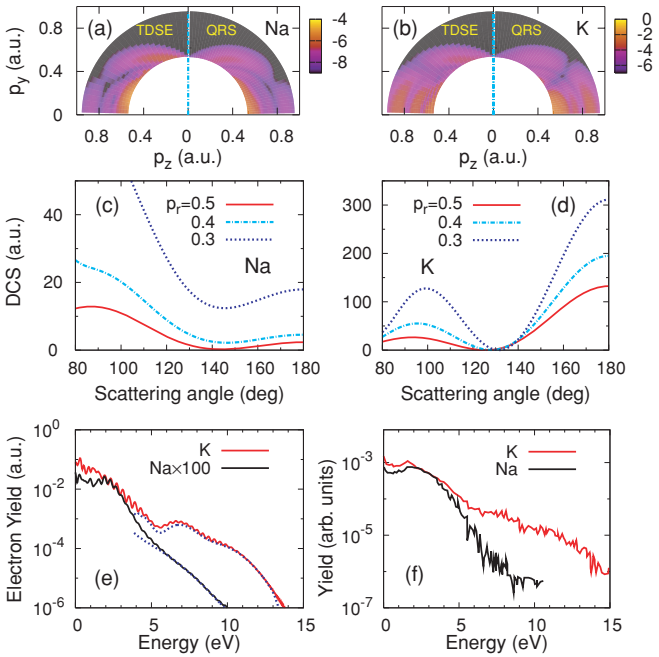

Figure 2. Single ionization of Na and K atoms by a five-cycle, 3.2 μm infrared laser with a peak intensity of 1.0×10^{12} W cm^{-2} ($U_p = 0.96$ eV). (a), (b) Comparison of 2D momentum distributions (in logarithmic scale) above $4U_p$ and $p_z \geqslant 0$ obtained from the TDSE with those from the QRS model. (c), (d) Electron–ion elastic DCS at large angles. (e) Angle-integrated electron energy spectra calculated from the TDSE (long solid lines from 0 to $15U_p$) and those from the QRS model (dotted lines above $4U_p$) for each target. (f) Experimental angle-integrated electron spectra taken from Gaarde *et al* [2]. In (e) and (f), the electron spectra from the two targets are normalized to each other at low energies.

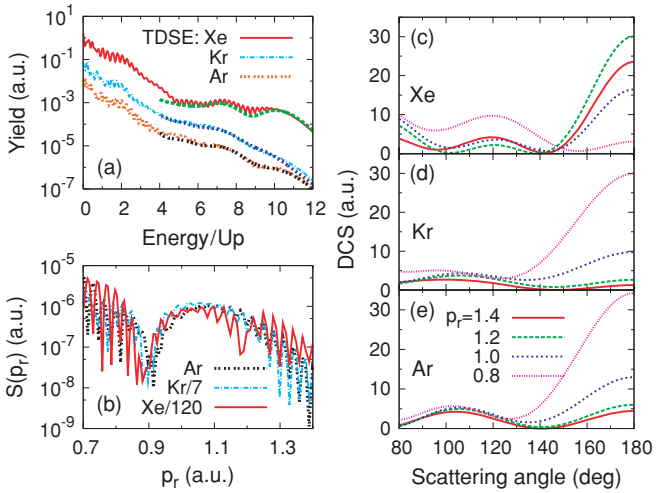

Figure 3. Single ionization of Xe, Kr and Ar atoms by a five-cycle laser pulse with a wavelength of 800 nm and a peak intensity of $I_0 = 1.0 \times 10^{14}$ W cm^{-2} ($A_0 = 0.94$). (a) Comparison of the angle-integrated electron energy spectra from the TDSE (long lines from 0 to $12U_p$) and from the QRS model (short lines above $4U_p$). The QRS energy spectra for Kr and Xe are calculated using the wave packet extracted from Ar, with proper normalization at one energy point. (b) Normalized momentum distributions of the returning electron wave packets extracted from the 'left side' ($p_z < 0$) of the momentum spectra. (c)–(e) Electron–ion elastic scattering DCS used in the QRS model.

In figures 2(c) and (d), the DCSs for e–Na$^+$ and e–K$^+$ collisions are shown for the range of momenta p_r that contribute to the plateau photoelectrons. In figure 2(e), the photoelectron energy spectra for sodium and potassium are shown. Note that in the plateau region, the QRS results agree quite well with those obtained from the TDSE. The spectra of the two targets are normalized to each other at low energies. The figure shows that potassium has a much higher and flatter plateau. This is easily understood using the QRS model since the DCS is much larger, especially at large θ, in potassium than in sodium; see figures 2(c) and (d). The electron spectra in figure 2(e) can also be compared to the experimental data reported in [2], as shown in figure 2(f). There is a close similarity in the relative yields between our calculations and experiment, even though our calculations used a five-cycle (20 fs FWHM) pulse while the experiment used somewhat different intensities for a pulse with a duration of 1.9 ps. Note that the pulse duration does not affect the relative energy dependence of the electron spectra if the interference features are smoothed out.

As a side note, we comment that the lower end of the plateau electrons has been set at $4U_p$ in this communication. According to the classical theory, direct ionization by tunnelling (without rescattering) will give a maximum electron energy of $2U_p$. Between 2 and $4U_p$, the direct ionization part could still interfere with the rescattering part [14]; thus, we chose $4U_p$ as the lower end of the QRS model.

We have also studied the plateau electrons in ATI for Ar, Kr and Xe atoms. Experimental data for these systems have been reported using lasers of different wavelengths and pulse durations since the 1990s [3, 4]. In figure 3(a), we show the calculated ATI spectra versus electron energy in units of U_p at the same laser intensity of 1.0×10^{14} W cm^{-2} for a five-cycle, 800 nm pulse. In the case of Xe, a clear flat plateau is seen—the yield remains almost constant from $5U_p$ to $10U_p$. For Kr and Ar, their yields drop about two to three orders of magnitude in the same energy range. Since the momentum distributions of the returning electron wave packets are essentially identical (up to a normalization due to the different tunnelling ionization rates) for the same laser pulse, as shown in figure 3(b), the differences in the electron energy spectra are attributed to the DCS among the three targets. In figures 3(c)–(e), their DCSs are shown for the relevant range of p_r. While they are in the same range of magnitude, at large angles θ, say 160°–180°, the DCS for Xe behaves 'anomalously', i.e. it increases with increasing energies instead of otherwise, as in Ar and Kr. Since electrons of higher returning energies contribute more to the plateau electron yields (see figure 1), this 'anomalous' energy dependence explains why Xe has a much flatter plateau. On the other hand, the 'normal' energy dependence (decreases with increasing energies) of the DCS in Ar and Kr explains why the electron yields drop steeply at high energies; see figure 3(a). We comment that the QRS results (curves that start from $4U_p$) shown in figure 3(a) are again in good agreement with those obtained from the TDSE.

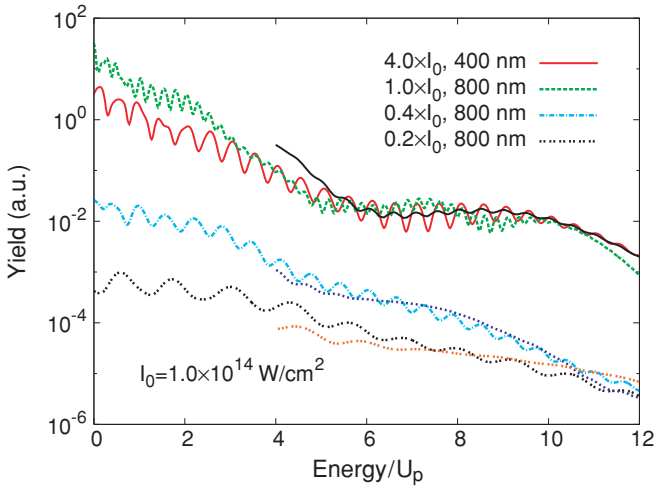

Figure 4. Comparison of the angle-integrated electron energy spectra from the TDSE (long lines from 0 to $12U_p$) and from the QRS model (short lines above $4U_p$) for single ionization of Xe atoms by five-cycle laser pulses at different laser intensities and with different wavelengths indicated in the figure. Note that the QRS model fails at the lowest intensity $0.2I_0$. See text.

According to the rescattering model, different lasers with identical U_p will generate returning electrons with the same range of kinetic energy. In figure 4, on the top set of curves, we show the photoelectron spectra for Xe using 800 nm and 400 nm lasers, respectively, but with the latter having four times the peak intensity of $I_0 = 1.0 \times 10^{14}$ W cm^{-2}. The spectra in the plateau region indeed agree quite well quantitatively after they are normalized to each other at around $10U_p$ (the two long lines on the top). Both results are obtained by solving the TDSE. The QRS results for 800 nm (the short solid line above $4U_p$) are also shown in the plateau region.

Since the QRS theory is based on the rescattering model, it is expected to fail at lower intensities in the multiphoton ionization regime. In figure 4, we compare TDSE and QRS results at two lower laser intensities of $0.4I_0$ and $0.2I_0$, with Keldysh parameters of $\gamma = 1.59$ and 2.24, respectively. We see evidence of the deviation of the QRS model from the TDSE (different slope) at $\gamma = 2.24$.

The above examples illustrate that the energy dependence of plateau photoelectrons above $4U_p$ is determined *entirely* by electron–ion elastic differential scattering cross sections. A flat plateau is expected if the DCS at large angles (close to 180°) increases with increasing electron energy and when the DCS is highly peaked at large angles, as in the case of Xe (figure 3(c)). Such conditions occur frequently in the DCS for low-energy electron–ion and electron–atom collisions. The energies where this occurs depend on the target species, and thus the behaviour of the plateau electrons depends on the laser intensity and the species. If the DCS is calculated by approximating the continuum electrons by plane waves or Coulomb waves, no flat plateau like that in Xe will ever appear since the DCS from these models decreases monotonically with increasing electron energy and scattering angles. The QRS theory also predicts that a flat plateau will not appear for an atomic hydrogen target for any intensity or wavelength of the lasers used because the corresponding DCS is given by the monotonic Rutherford formula. Indeed, an early experiment did show that atomic hydrogen does not have a flat high-energy plateau [21].

In summary, we showed that the species dependence of laser-generated high-energy plateau electrons is directly related to the behaviour of the elastic scattering DCS between the returning electrons with the target ion. Together with our previous results where the species dependence of HHG was traced to their photo-recombination cross sections [15, 22, 23], we have now established a QRS theory for the ATI electron and HHG spectra in each of their respective plateau regions. As shown elsewhere [14, 23], the 'wave packet' can be extracted from a companion target or from the second-order strong field approximation [14] where the electron–ion interaction is only treated to the first order. Thus, according to the QRS theory, the calculation of the nonlinear HHG is reduced to the calculation of photo-recombination cross sections, and the calculation of plateau electrons is reduced to the calculation of the electron–ion elastic scattering DCS. The QRS theory allows one to bypass the need of solving the TDSE for complex systems. Conversely, the QRS theory also allows one to extract electron and photon scattering information from experimental high-energy photoelectron spectra or HHG. As proposed elsewhere [24], these cross sections can be further used to deduce the structure of the target, thus opening up the opportunity of using infrared laser pulses for determining the structural change of a dynamic system with temporal resolution of sub-femtoseconds to a few femtoseconds.

Acknowledgments

This work was supported in part by Chemical Sciences, Geosciences and Biosciences Division, Office of Basic Energy Sciences, Office of Science, US Department of Energy. TM is also supported by a Grant-in-Aid for Scientific Research (C) from MEXT, Japan, and by a JSPS Bilateral joint program between US and Japan.

References

[1] Agostini P, Fabre F, Mainfray G and Petite G 1979 *Phys. Rev. Lett.* **42** 1127
[2] Gaarde M B, Schafer K J, Kulander K C, Sheehy B, Kim D and DiMauro L F 2000 *Phys. Rev. Lett.* **84** 2822
[3] Paulus G G, Nicklich W, Xu H, Lambropoulos P and Walther H 1994 *Phys. Rev. Lett.* **72** 2851
[4] Grasbon F, Paulus G G, Walther H, Villoresi P, Sansone G, Stagira S, Nisoli M and Silvestri S D 2003 *Phys. Rev. Lett.* **91** 173003
[5] Yang B, Schafer K J, Walker B, Kulander K C, Agostini P and DiMauro L F 1993 *Phys. Rev. Lett.* **71** 3770
[6] Paulus G G, Becker W, Nicklich W and Walther H 1994 *J. Phys. B: At. Mol. Phys.* **27** L703
[7] Walker B, Sheehy B, Kulander K C and DiMauro L F 1996 *Phys. Rev. Lett.* **77** 5031
[8] Kroll N M and Watson K M 1973 *Phys. Rev.* A **8** 804
[9] Gallagher T F 1988 *Phys. Rev. Lett.* **61** 2304
[10] Krause J L, Schafer K J and Kulander K C 1992 *Phys. Rev. Lett.* **68** 3535

[11] Corkum P B 1993 *Phys. Rev. Lett.* **71** 1994
[12] Milošević D B, Paulus G G, Bauer D and Becker W 2006 *J. Phys. B: At. Mol. Opt. Phys.* **39** R203
[13] Bauer D 2005 *Phys. Rev. Lett.* **94** 113001
[14] Chen Z, Morishita T, Le A T and Lin C D 2007 *Phys. Rev.* A **76** 043402
[15] Morishita T, Le A T, Chen Z and Lin C D 2008 *Phys. Rev. Lett.* **100** 013903
[16] Morishita T, Chen Z, Watanabe S and Lin C D 2007 *Phys. Rev.* A **75** 023407
[17] Schiff L I 1968 *Quantum Mechanics* 3rd edn (New York: McGraw-Hill) p 145
[18] Okunishi M, Morishita T, Prümper G, Shimada K, Lin C D, Watanabe S and Ueda K 2008 *Phys. Rev. Lett.* **100** 143001
[19] Ray D *et al* 2008 *Phys. Rev. Lett.* **100** 143002
[20] Lewenstein M, Balcou P, Ivanov M Y, L'Huillier A and Corkum P B 1994 *Phys. Rev.* A **49** 2117
[21] Paulus G G, Nicklich W, Zacher F, Lambropoulos P and Walther H 1996 *J. Phys. B: At. Mol. Opt. Phys.* **29** L249
[22] Le A T, Picca R D, Fainstein P D, Telnov D A, Lein M and Lin C D 2008 *J. Phys. B: At. Mol. Opt. Phys.* **41** 081002
[23] Le A T, Morishita T and Lin C D 2008 *Phys. Rev.* A **78** 023814
[24] Morishita T, Le A T, Chen Z and Lin C D 2008 *New J. Phys.* **10** 025011